

## QUASI-PERIODIC OSCILLATIONS AS GLOBAL HYDRODYNAMIC MODES IN THE BOUNDARY LAYERS OF VISCOUS ACCRETION DISKS

M. HAKAN ERKUT,<sup>1,2</sup> DIMITRIOS PSALTIS,<sup>2,3</sup> AND M. ALI ALPAR<sup>3</sup><sup>1</sup>Department of Mathematics and Computer Science, İstanbul Kültür University, Ataköy Campus, Bakırköy 34156, İstanbul, Turkey<sup>2</sup>Physics Department, University of Arizona, 1118 E. 4th St., Tucson, AZ 85721 and<sup>3</sup>Faculty of Engineering and Natural Sciences, Sabancı University, 34956, Orhanlı, Tuzla, İstanbul, Turkey

## ABSTRACT

The observational characteristics of quasi-periodic oscillations (QPOs) from accreting neutron stars strongly indicate the oscillatory modes in the innermost regions of accretion disks as a likely source of the QPOs. The inner regions of accretion disks around neutron stars can harbor very high frequency modes related to the radial epicyclic frequency  $\kappa$ . The degeneracy of  $\kappa$  with the orbital frequency  $\Omega$  is removed in a non-Keplerian boundary or transition zone near the magnetopause between the disk and the compact object. We show, by analyzing the global hydrodynamic modes of long wavelength in the boundary layers of viscous accretion disks, that the fastest growing mode frequencies are associated with frequency bands around  $\kappa$  and  $\kappa \pm \Omega$ . The maximum growth rates are achieved near the radius where the orbital frequency  $\Omega$  is maximum. The global hydrodynamic parameters such as the surface density profile and the radial drift velocity determine which modes of free oscillations will grow at a given particular radius in the boundary layer. In accordance with the peak separation between kHz QPOs observed in neutron-star sources, the difference frequency between two consecutive bands of the fastest growing modes is always related to the spin frequency of the neutron star. This is a natural outcome of the boundary condition imposed by the rotating magnetosphere on the boundary region of the inner disk.

*Subject headings:* accretion, accretion disks — stars: neutron — stars: oscillations — X-rays: stars

## 1. INTRODUCTION

Wave modes in the boundary region in the inner accretion disk are a likely source of the distinct narrow frequency bands of quasi-periodic oscillations (QPOs) (van der Klis 2000) from neutron star sources in low mass X-ray binaries (LMXBs). The dependence of QPO frequencies on accretion rate suggests that the observed QPOs are connected with accretion disk modes. Psaltis, Belloni & van der Klis (1999) showed the existence of correlations between the frequencies of different QPO bands extending over a wide span of frequencies. The same correlation encompasses black hole as well as white dwarf and neutron star sources. This strongly implies that the frequency bands are determined by the oscillation modes of the accretion disk. The nature of the compact object, whether it is a black hole, white dwarf or neutron star, probably plays a role in exciting the same disk modes through possibly different mechanisms in different types of compact sources. The QPO bands modifying the X-ray luminosity are likely to belong to the boundary region between the disk and the compact object. For magnetic neutron stars, this boundary region is shaped by the interaction of the disk with the magnetosphere. The region where the rotation deviates from Keplerian flow is not necessarily very narrow; this boundary zone may have a size as large as a few tenths of the inner disk radius. We shall therefore use the terms “boundary” and “transition” region interchangeably.

Initial explorations of disk modes underlying QPO frequency bands from LMXBs were provided by Alpar et al. (1992) and Alpar & Yılmaz (1997). The characteristics and possible excitation mechanisms of thin-disk oscillations were reviewed and discussed by Kato (2001). In many current models of QPOs, especially those of neutron stars, their fre-

quencies are identified with test-particle frequencies (Stella, Vietri & Morsink 1999; Abramowicz et al. 2003). Most parts of an accretion disk, except, significantly, the transition regions at the inner boundary of the disk, are characterized by Keplerian rotation rates to a very good approximation. At any radius beyond the transition region, acoustic, magneto-acoustic and viscous corrections to the test-particle Keplerian orbital frequency are negligible. In the outer disk regime for disks around neutron stars and white dwarfs (and far enough from a central black hole), test-particle frequencies for radial and vertical perturbations of the orbit are degenerate with the Keplerian orbital frequency. The degeneracy is removed if the effects of general relativity are important. A Newtonian field of tidal or higher multi-pole structure would also lead to a split in the degeneracy. However, in Newtonian gravity, distortions of stellar shape even for the most rapidly rotating neutron stars will not introduce a significant level of non-degeneracy between the frequencies of test-particle oscillations that is comparable to the difference between the observed QPO frequency bands. Models employing the Keplerian frequency have been relatively successful in interpreting QPO frequency correlations. The Kepler (test particle) frequency interpretation has also been employed to place constraints on the masses and spins of compact objects. Empirically, predictions based on test-particle frequencies applied to QPO frequency correlations deviate from observations at a level of about 10%.

The Keplerian frequency represents the basic imprint of rotation on all the dynamical responses of the disk. Albeit simple, the identification of QPOs with test-particle frequencies has a number of shortcomings. First, precisely in a boundary layer where QPOs are expected to be excited, the dynamical frequencies of oscillations are not the test-particle frequencies. In the boundary layer, viscous and magnetic forces lead to deviation of orbital frequencies from Keplerian test-

<sup>1</sup> m.erkut@iku.edu.tr<sup>2</sup> dpsaltis@physics.arizona.edu<sup>3</sup> alpar@sabanciuniv.edu

particle frequencies (see, e.g., Erkut & Alpar 2004). The resulting band of non-Keplerian rotation frequencies entail viscous and acoustic response and couplings between adjacent rings of the disk fluid. Hydrodynamic effects are therefore essential for an understanding of the frequency bands characterizing the boundary layer. In particular, the degeneracy of test-particle frequencies in the non-relativistic regime is lifted in the hydrodynamic boundary layer, where the radial epicyclic frequency is in fact larger than the orbital frequency. This simple observation (Alpar & Psaltis 2005) has important consequences for the interpretation of kHz QPO frequencies, in particular for the constraints on the neutron star mass-radius relation derived from kHz QPOs.

Second, test-particle frequencies do not distinguish between azimuthal sidebands. While kinematic models of QPOs like the beat-frequency model involve one specific band of frequencies, say  $\omega$ , a large number of sidebands, of frequencies  $\omega_m \cong \omega - m\Omega$ , where  $\Omega$  is the orbital frequency, are allowed by azimuthal symmetry. Arguments as to why only one or two QPO bands are excited must involve choices imposed by the symmetries of the interaction between the magnetosphere and the accretion disk boundary, leading to resonances with particular frequencies at one or more radial regions in the disk. Without resonances, test-particle frequency spectra present no distinction between the modes. The realistic hydrodynamic modes may, in some parameter ranges, distinguish between both fundamental modes and all their azimuthal sidebands through the different growth or decay rates of these modes, *even in the case of free oscillations*. A reduction of the number of relevant (easily excitable) modes of free oscillations is certainly an important task for an understanding of accretion disks around neutron stars, white dwarfs and black holes. In the case of black holes, this classification of free hydrodynamic modes in terms of their growth rates is even more important as resonant excitation by the black hole is not available.

In this paper, we study the global modes of free oscillations at some position  $r$  in the inner disk-boundary or transition region by analyzing the perturbed dynamical equations of a hydrodynamic disk, including pressure gradients, viscous and magnetic stresses. We consider the case of a disk around a neutron star with a magnetosphere. The neutron star is taken to be a *slow rotator*: the star's rotation rate is less than the value of the Keplerian rotation rate at the inner radius of the disk;  $\Omega_* < \Omega_K(r_{\text{in}})$ . The actual rotation rate of the disk is set by the boundary condition  $\Omega(r_{\text{in}}) = \Omega_*$ . Thus in the steady state solutions for the disk, the rotation rate at the inner edge of the disk and in the transition region beyond is sub-Keplerian. The innermost disk radius  $r_{\text{in}}$  determines the disk magnetosphere interface which may be subject to magnetic Rayleigh-Taylor or interchange instabilities. This instability operates mainly at the disk-magnetosphere interface because of the sharp density contrast across the radius  $r = r_{\text{in}}$ . The inner disk region for  $r \gtrsim r_{\text{in}}$  consists of a non-Keplerian boundary region that joins the outer Keplerian disk with a continuous density distribution. As we will see in § 3.2, the surface density profile throughout the non-Keplerian boundary region increases with decreasing radii. Thus, our boundary region is not subject to interchange-like instabilities.

The free oscillation modes we explore by perturbing a steady state solution embody information about the stability of the disk through their growth or decay rates. Growing modes will provide a clue as to the origin of the QPO frequency bands, which could be excited by resonant forcing of

the disk by time dependent interactions with the star's magnetosphere. We find, as expected, that growth or decay rates are determined by the dynamical effects of viscosity, with an additional dependence on the sound speed and the density and rotation-rate profiles in the non-Keplerian boundary region. For some boundary region parameters, not all fundamental modes of free oscillations and not all azimuthal sidebands grow, and among the growing modes the growth rates differ. For other choices of boundary region parameters the growth rates of all sidebands are similar. The frequencies of the modes differ from test-particle frequencies by amounts that can be several times larger than the corresponding QPO width. Most importantly, for a reasonable set of accretion disk parameters, we can show that only a certain few of the hydrodynamic free oscillation modes will grow, and that the frequency bands of these oscillations can be associated with the observed frequency bands. The nature of free oscillation modes in the boundary region depends on whether the neutron star is rotating at a rate slower or faster than the rotation rates prevailing in the inner boundary of the disk. In this paper, we will consider the more common and straightforward case of *slow rotators*, the case when the neutron star rotation rate  $\Omega_*$  is less than  $\Omega_K(r_{\text{in}})$ , the Kepler rotation rate at some representative inner disk radius  $r_{\text{in}}$ . An investigation of *forced* resonant excitation of these prevalent modes, and the comparison and association with observed QPO bands will follow in a subsequent paper.

§ 2 lays out the basic assumptions and equations, § 3 displays the mode analysis for the free oscillations, including a discussion of hydrodynamic effects, frequency bands, and growth rates. In § 4, we discuss the results and present our conclusions.

## 2. BASIC EQUATIONS AND ASSUMPTIONS

We consider the excitation of oscillations in a geometrically thin disk in vertical hydrostatic equilibrium. We write the continuity and the radial and angular momentum equations in cylindrical coordinates, integrated vertically over the disk thickness, as

$$\frac{\partial \Sigma}{\partial t} + \frac{1}{r} \frac{\partial}{\partial r} (r \Sigma v_r) + \frac{1}{r} \frac{\partial}{\partial \phi} (\Sigma v_\phi) = 0, \quad (1)$$

$$\frac{\partial v_r}{\partial t} + v_r \frac{\partial v_r}{\partial r} + \frac{v_\phi}{r} \frac{\partial v_r}{\partial \phi} - \frac{v_\phi^2}{r} = - \left( \frac{\partial \Phi}{\partial r} \right)_{z=H} - \frac{1}{\Sigma} \frac{\partial \Pi}{\partial r} + \langle F_r \rangle, \quad (2)$$

and

$$\frac{\partial v_\phi}{\partial t} + v_r \frac{\partial v_\phi}{\partial r} + \frac{v_\phi}{r} \frac{\partial v_\phi}{\partial \phi} + v_r \frac{v_\phi}{r} = - \frac{1}{\Sigma r} \frac{\partial \Pi}{\partial \phi} + \langle F_\phi \rangle. \quad (3)$$

Here,  $H$  is the half-thickness of the disk,  $v_r$  and  $v_\phi$  are the radial and azimuthal components of the velocity field in the disk,  $\Phi$  is the gravitational potential,

$$\Sigma \equiv \int_{-H}^H \rho dz \quad (4)$$

is the surface mass density,

$$\Pi \equiv \int_{-H}^H P dz \quad (5)$$

is the vertically integrated thermal pressure,  $\rho$  is the mass density,  $P$  is the sum of the gas and radiation pressures, and

$$\langle F_j \rangle \equiv \frac{1}{\Sigma} \int_{-H}^H F_j \rho dz \quad (6)$$

are the vertically averaged sums of the magnetic and viscous forces per unit mass, and the subscript  $j$  stands for the  $r$  or  $\phi$  component of the force.

We only consider the  $\phi$ -component of the viscous force as the dominant shear stress between adjacent layers, because of our assumption that the disk is geometrically thin (Shakura & Sunyaev 1973). We write the sum of the viscous and large-scale magnetic forces (per unit mass) in the radial and azimuthal directions as  $F_r = F_r^{\text{mag}}$  and  $F_\phi = F_\phi^{\text{vis}} + F_\phi^{\text{mag}}$ , respectively.

The steady, axisymmetric, equilibrium state obeys

$$-2\pi r \Sigma_0 v_{r0} = \dot{M}, \quad (7)$$

$$v_{r0} \frac{dv_{r0}}{dr} - \Omega^2 r = - \left( \frac{\partial \Phi}{\partial r} \right)_{z=H} - \frac{1}{\Sigma_0} \frac{d\Pi_0}{dr} + \langle F_r^{\text{mag}} \rangle_0, \quad (8)$$

and

$$\frac{\kappa^2}{2\Omega} v_{r0} = \langle F_\phi^{\text{vis}} \rangle_0 + \langle F_\phi^{\text{mag}} \rangle_0, \quad (9)$$

where  $\dot{M}$  is the constant mass-inflow rate,  $v_{r0} < 0$ ,  $v_{\phi0} = \Omega r$ ,  $\Omega$  is the angular velocity of the disk plasma, and  $\kappa \equiv [2\Omega(2\Omega + r d\Omega/dr)]^{1/2}$  is the radial epicyclic frequency.

We introduce perturbations to this axisymmetric fluid distribution and use the subscripts “0” and “1” to denote the equilibrium and perturbed states, respectively. The linearized perturbation equations follow from equations (1)–(3) as

$$\frac{d\Sigma_1}{d\tau} + \frac{1}{r} \frac{\partial}{\partial r} [r(\Sigma_0 v_{r1} + \Sigma_1 v_{r0})] + \frac{1}{r} \frac{\partial}{\partial \phi} (\Sigma_0 v_{\phi1}) = 0, \quad (10)$$

$$\begin{aligned} \frac{dv_{r1}}{d\tau} - 2\Omega v_{\phi1} + \frac{\partial}{\partial r} (v_{r0} v_{r1}) &= \frac{1}{\Sigma_0} \left( \frac{\Sigma_1}{\Sigma_0} \frac{d\Pi_0}{dr} - \frac{\partial \Pi_1}{\partial r} \right) \\ &+ \langle F_r^{\text{mag}} \rangle_1, \end{aligned} \quad (11)$$

and

$$\begin{aligned} \frac{dv_{\phi1}}{d\tau} + \frac{\kappa^2}{2\Omega} v_{r1} + \frac{v_{r0}}{r} v_{\phi1} + v_{r0} \frac{\partial v_{\phi1}}{\partial r} &= - \frac{1}{\Sigma_0 r} \frac{\partial \Pi_1}{\partial \phi} + \langle F_\phi^{\text{vis}} \rangle_1 \\ &+ \langle F_\phi^{\text{mag}} \rangle_1, \end{aligned} \quad (12)$$

where  $d/d\tau \equiv \partial/\partial t + \Omega \partial/\partial \phi$  is the Lagrangian derivative following the motion of the fluid in the azimuthal direction.

In the following, we study perturbations varying on timescales shorter than the thermal timescale and thus expect that there is no energy exchange between adjacent fluid elements. In this case, the fluid elements respond adiabatically to density and pressure perturbations and, at the same time, the disk thickness  $H$ , which is determined by vertical hydrostatic equilibrium, responds to the change of pressure. In general, we can write (Stehle & Spruit 1999)

$$\Pi_1 = \Sigma_1 \left( \frac{\Pi_0}{\Sigma_0} \right) \left( \Gamma + \frac{\partial \ln H}{\partial \ln \rho} \right), \quad (13)$$

where  $\Gamma$  is the index of a polytropic equation of state. The terms in the last parenthesis is of order unity. Because we will not be calculating explicitly changes in the vertical equilibrium during the oscillations, we will set the last term to unity. Therefore, we will be studying effectively isothermal modes.

We consider long wavelength perturbations to analyze the lowest order normal modes extending globally over the radial distance scale  $r_{\text{out}}$  of the disk. For the stability of such global modes the effect of cylindrical geometry and of the structure

of the unperturbed disk state must be taken into account. We perform a local mode analysis. Our approach differs from the usual local mode analysis of short-wavelength perturbations of radial dependence  $e^{ikr}$  in a WKB approximation. Consideration of modes with radial wavenumbers would be appropriate for the analysis of local disk modes in the short wavelength regime. Instead, we study the stability of the global disk modes at each particular radius  $r$  in the boundary layer. In this region, the unperturbed disk quantities such as the surface density  $\Sigma_0$  and the rotation rate  $\Omega$  change on a length scale  $(\Delta r)_{\text{BL}} < r_{\text{in}}$ . Since the variation of the global long wavelength perturbations has a much longer range  $r_{\text{out}} \gg (\Delta r)_{\text{BL}}$  in the radial direction, we write equations (10)–(12) at any particular radius  $r$  in dimensionless form, neglecting the  $r$ -dependence of the perturbations:

$$\frac{d\sigma}{d\tau} + (1 + \beta)\Omega_s u_r + \beta\Omega_\nu \sigma + \Omega_s \frac{\partial u_\phi}{\partial \phi} = 0, \quad (14)$$

$$\frac{du_r}{d\tau} - 2\Omega u_\phi + (1 + \beta)\Omega_\nu u_r = \beta\Omega_s \sigma + f_r^{\text{mag}}, \quad (15)$$

$$\frac{du_\phi}{d\tau} + \frac{\kappa^2}{2\Omega} u_r - \Omega_\nu u_\phi = -\Omega_s \frac{\partial \sigma}{\partial \phi} + f_\phi^{\text{vis}} + f_\phi^{\text{mag}}. \quad (16)$$

Here,  $\sigma \equiv \Sigma_1/\Sigma_0$  is the dimensionless density perturbation,  $u_r \equiv v_{r1}/c_s$  and  $u_\phi \equiv v_{\phi1}/c_s$  are the dimensionless velocity perturbations,  $f_{r,\phi} \equiv \langle F_{r,\phi} \rangle_1/c_s$  are the force perturbations in units of frequency, and  $\Omega_\nu \equiv -v_{r0}/r$  and  $\Omega_s \equiv c_s/r$  are the typical frequencies associated with the radial accretion and the effective sound speed  $c_s = (\Pi_0/\Sigma_0)^{1/2}$ , respectively. The parameter

$$\beta \equiv \left( \frac{d \ln \Sigma_0}{d \ln r} \right)_r \quad (17)$$

represents the surface mass density profile at a particular radius  $r$  in the inner disk. Note that  $\beta$  crucially represents the structure of the unperturbed disk. This differs from the usual local mode analysis in which the radial variation of the unperturbed background quantities such as  $\Sigma_0$  is neglected while the radial derivatives of the perturbations are taken into account in terms of their radial wavenumbers.

We look for solutions of the above linear set of equations of the form

$$q(\phi, t) = \sum_m \int q_m(\omega) e^{i(m\phi - \omega t)} d\omega, \quad (18)$$

where the integer  $m \geq 1$  represents non-axisymmetric modes corresponding to the prograde motion of perturbations in the azimuthal direction. The Fourier decomposition of equations (14)–(16) yields

$$[i(m\Omega - \omega) + \beta\Omega_\nu] \sigma_m + (1 + \beta)\Omega_s u_{r,m} + im\Omega_s u_{\phi,m} = 0, \quad (19)$$

$$-\beta\Omega_s \sigma_m + [i(m\Omega - \omega) + (1 + \beta)\Omega_\nu] u_{r,m} - 2\Omega u_{\phi,m} = f_{r,m}^{\text{mag}}, \quad (20)$$

$$im\Omega_s \sigma_m + \frac{\kappa^2}{2\Omega} u_{r,m} + [i(m\Omega - \omega) - \Omega_\nu] u_{\phi,m} = f_{\phi,m}^{\text{vis}} + f_{\phi,m}^{\text{mag}}. \quad (21)$$

To proceed further in the linear mode analysis, we need to specify the force perturbations  $f_{r,m}$  and  $f_{\phi,m}$  in equations (20) and (21).

In this paper, we discuss the free oscillation modes. In a subsequent paper, we will study oscillations forced by external perturbations, as in the case of a compact object with an oblique large-scale magnetic field.

## 3. GLOBAL FREE OSCILLATIONS IN A VISCOUS ACCRETION DISK

When there are no perturbations introduced by large-scale magnetic fields, i.e., when  $f_{r,m}^{\text{mag}} = f_{\phi,m}^{\text{mag}} = 0$ , the only non-negligible force perturbation is due to the kinematic viscosity  $\nu$ . In the absence of an analytic model for the effective kinematic viscosity in a turbulent shearing flow, we adopt a simple damping force prescription, i.e.,  $F_{\phi}^{\text{vis}} = -\nu_{\phi}/t_{\nu}$ , where  $t_{\nu}$  is the timescale for viscous accretion. In order for our prescription to yield the order-of-magnitude estimate for the viscous timescale,  $t_{\nu} \sim r^2/\nu \sim r/|v_{r0}|$ , we write

$$\langle F_{\phi}^{\text{vis}} \rangle = \gamma_{\nu} \frac{v_{r0} v_{\phi}}{r}, \quad (22)$$

where  $\gamma_{\nu}$  is a dimensionless factor. Note that, for this prescription of the viscous force to satisfy equation (9) for the steady equilibrium state, it is necessary that

$$\gamma_{\nu} = \frac{\kappa^2}{2\Omega^2} - \frac{\langle F_{\phi}^{\text{mag}} \rangle_0}{v_{r0}\Omega}. \quad (23)$$

To linear order in the perturbed quantities, equation (22) yields  $\langle F_{\phi} \rangle_1 = -\gamma_{\nu} \Omega_{\nu} v_{\phi 1}$ . The zeroth-order magnetic force enters the perturbation equations only through the parameter  $\gamma_{\nu}$  as given in equation (23).

For the case of interest, equations (19)–(21) become

$$[i(m\Omega - \omega) + \beta\Omega_{\nu}] \sigma_m + (1 + \beta)\Omega_s u_{r,m} + im\Omega_s u_{\phi,m} = 0, \quad (24)$$

$$-\beta\Omega_s \sigma_m + [i(m\Omega - \omega) + (1 + \beta)\Omega_{\nu}] u_{r,m} - 2\Omega u_{\phi,m} = 0, \quad (25)$$

$$im\Omega_s \sigma_m + \frac{\kappa^2}{2\Omega} u_{r,m} + [i(m\Omega - \omega) - (1 - \gamma_{\nu})\Omega_{\nu}] u_{\phi,m} = 0, \quad (26)$$

yielding a dispersion relation of third order in  $\omega$ . We provide the general expressions for the dispersion relation and the three complex solutions in the Appendix.

For illustrative purposes, we write the expressions for the three frequencies to leading order in  $\Omega_s/\Omega$ , i.e., for small hydrodynamic corrections. The solutions of astrophysical interest may actually be found in situations beyond this approximate regime, as we shall discuss in § 3.2. However, the approximate solutions shed light on the basic parameters that determine the frequencies and growth rates of the modes. In the limit of small hydrodynamic corrections, i.e.  $\varepsilon_1, \varepsilon_2$ , and  $\varepsilon_3 \ll 1$  (see Appendix), the axisymmetric modes ( $m = 0$ ) have the frequencies and growth rates

$$\begin{aligned} \text{Re} [\omega_{1,2}^{(0)}] &= \pm \kappa \pm \beta(1 + \beta) \left( \frac{\Omega_s}{2\kappa} \right) \Omega_s \\ &\pm \left[ 3(\gamma_{\nu} - \beta - 1) - (\gamma_{\nu} - \beta)^2 \right] \left( \frac{\Omega_{\nu}}{6\kappa} \right) \Omega_{\nu}, \end{aligned} \quad (27)$$

$$\text{Im} [\omega_{1,2}^{(0)}] = - \left( \frac{\gamma_{\nu} + \beta}{2} \right) \Omega_{\nu}, \quad (28)$$

$$\text{Re} [\omega_3^{(0)}] = 0, \quad (29)$$

and

$$\text{Im} [\omega_3^{(0)}] = -\beta\Omega_{\nu}. \quad (30)$$

The corresponding expressions for the non-axisymmetric modes, with positive or negative integer values of the azimuthal wavenumber  $m$  are

$$\begin{aligned} \text{Re} [\omega_{1,2}^{(m)}] &= m\Omega \pm \kappa \pm [m^2 + \beta(1 + \beta)] \left( \frac{\Omega_s}{2\kappa} \right) \Omega_s \\ &\pm \left[ 3(\gamma_{\nu} - \beta - 1) - (\gamma_{\nu} - \beta)^2 \right] \left( \frac{\Omega_{\nu}}{6\kappa} \right) \Omega_{\nu}, \end{aligned} \quad (31)$$

$$\text{Im} [\omega_{1,2}^{(m)}] = - \left( \frac{\gamma_{\nu} + 2\beta}{3} \right) \Omega_{\nu}, \quad (32)$$

$$\text{Re} [\omega_3^{(m)}] = m\Omega, \quad (33)$$

and

$$\text{Im} [\omega_3^{(m)}] = - \left( \frac{\gamma_{\nu} + 2\beta}{3} \right) \Omega_{\nu}. \quad (34)$$

Modes whose real frequencies differ only by a sign are of course identical. We note that in these approximate expressions to leading order in  $\Omega_s$  the imaginary parts have no dependence on  $m$ . This means that the fundamental modes and the infinite sequence of sidebands shifted in frequency by  $\pm|m|\Omega$  from the fundamental modes of interest, all have the same growth or decay rates in the limit of small hydrodynamic corrections, i.e.  $\Omega_{\nu} \ll \Omega$  and  $\Omega_s \ll \Omega$ . Any distinction between the free oscillation modes arises only in a regime in which acoustic and viscous hydrodynamic effects are important.

It is possible to check the consistency of our stability analysis using equations (28), (30), (32), and (34) in the limit of non-magnetic local modes for which the radial gradient in the background surface density at any given location is negligible, that is,  $d \ln \Sigma_0 / d \ln r \ll 1$ . Note that none of the modes grows if the local gradient of the surface density is neglected ( $\beta = 0$ ) since  $\gamma_{\nu} > 0$  for  $\langle F_{\phi}^{\text{mag}} \rangle_0 = 0$ . There is no instability for local hydrodynamic modes in the long wavelength limit. The global modes grow in the inner disk where the radial gradient of  $\Sigma_0$  cannot be neglected ( $\beta \neq 0$ ).

## 3.1. Hydrodynamic Corrections to Test-particle Frequencies

In the ideal case of  $\Omega_{\nu} = \Omega_s = 0$ , the three characteristic frequencies coincide with appropriate combinations of test-particle frequencies in the disk, i.e.,  $\omega_1^{(m)} \simeq \kappa + |m|\Omega$ ,  $\omega_2^{(m)} \simeq \kappa - |m|\Omega$ , and  $\omega_3^{(m)} \simeq |m|\Omega$ . This justifies, to zeroth order, the identification of the observed QPO frequencies with frequencies of test particles in kinematic models of the QPOs. For example, in the sonic-point model (Miller et al. 1998), the higher kHz QPO would be the  $\omega_3^{(1)}$  mode at the sonic radius. In the relativistic precession model (Stella et al. 1999), the two high-frequency QPOs would be the  $\omega_3^{(1)}$  and  $\omega_2^{(1)}$  modes.

In the absence of external forcing, high-frequency modes in an accretion disk can be excited only in the presence of viscosity. This is a well-known result, discussed in detail by Kato (2001). Because the disk cannot respond thermally at the high-frequencies of interest here, viscosity can excite the modes only through its dynamical effect (mechanism II in Kato 2001) and not through its thermal effect (mechanism I in Kato 2001). Thus free oscillation modes in the accretion disk modes can have positive growth rates only if  $\Omega_{\nu}$  is not zero, i.e., through the effect of viscosity, and, hence, only if the hydrodynamic contributions to their frequencies are operative. Indeed, all models of hydrodynamic accretion disk modes show that non-negligible hydrodynamic corrections modify the test-particle frequencies of growing modes (see, e.g., Wagoner 1999; Kato 2001; Psaltis & Norman 2000).

We estimate the expected hydrodynamic corrections to the oscillatory mode frequencies typically identified with high-frequency QPOs using the scaling of the viscous and thermal frequencies in an alpha disk, i.e.,

$$\Omega_{\nu} \simeq \alpha \left( \frac{H}{r} \right)^2 \left( \frac{\Omega_K}{\Omega} \right)^2 \Omega \quad (35)$$

and

$$\Omega_s \simeq \left(\frac{H}{r}\right) \left(\frac{\Omega_K}{\Omega}\right) \Omega. \quad (36)$$

The fractional hydrodynamic correction to, e.g., the  $\text{Re}[\omega_2^{(1)}] \simeq \kappa - \Omega$  mode is determined by the acoustic response provided that  $\alpha$  is not close to unity:

$$\frac{\delta\omega_2^{(1)}}{\omega_2^{(1)}} \simeq \frac{\Omega_s^2}{\kappa(\kappa - \Omega)} \simeq \left(\frac{H}{r}\right)^2 \left(\frac{\kappa}{\Omega}\right)^{-1} \left(\frac{\Omega_K}{\Omega}\right)^2 \left|1 - \frac{\kappa}{\Omega}\right|^{-1}. \quad (37)$$

The growth rate of the same modes is  $\simeq \Omega_\nu$  and hence the quality factor  $Q$  of the corresponding QPO will be at most

$$Q \simeq \frac{\kappa - \Omega}{\Omega_\nu} \simeq \alpha^{-1} \left(\frac{H}{r}\right)^{-2} \left(\frac{\Omega_K}{\Omega}\right)^{-2} \left|1 - \frac{\kappa}{\Omega}\right| \quad (38)$$

and the resulting width of the QPO will be  $\simeq |\Omega - \kappa|/Q \simeq \Omega_\nu$ . Combining equations (37) and (38) we obtain for the hydrodynamic correction to the mode frequency in units of the width of the corresponding QPO the relation

$$\frac{\delta\omega_2^{(1)}}{\omega_2^{(1)}/Q} \simeq \frac{1}{\alpha} \left(\frac{\Omega}{\kappa}\right). \quad (39)$$

It is clear from this expression that, even for relatively large values of the parameter  $\alpha \simeq 0.1$ , the QPOs will have frequencies that are distinct from the corresponding test-particle frequencies by amounts that are several times larger than the QPO widths.

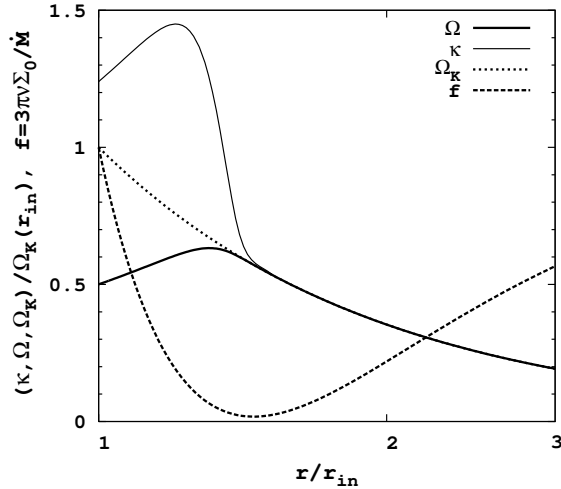


FIG. 1.— The radial profiles of the orbital frequency  $\Omega(r)$ , epicyclic frequency  $\kappa(r)$ , Keplerian frequency  $\Omega_K(r)$ , and the vertically integrated dynamical viscosity  $f(r)$  throughout the inner disk. This example is based on a typical boundary region model from Erkut & Alpar (2004). The frequencies are given in units of  $\Omega_K(r_{\text{in}})$ . In this particular example, the actual orbital frequency at the inner disk boundary and the rotation rate of the neutron star are half the Keplerian value at  $r_{\text{in}}$ ;  $\Omega(r_{\text{in}}) = \Omega_* = \Omega_K(r_{\text{in}})/2$ .

### 3.2. Excitation of Global Hydrodynamic Free Oscillation Modes

The growth rates of free oscillation modes are determined by a number of parameters characterizing the boundary region in the inner disk. In this region, the angular velocity of the disk matter makes a transition from the Keplerian rotation to match the stellar rotation rate. Our analysis depends on the local values of these parameters at any particular radius  $r$

within this transition or boundary region. The main parameters are the ratio of the radial epicyclic frequency  $\kappa$  to the orbital angular frequency  $\Omega$ , the radial surface-density profile  $\beta$  (equation 17),  $\Omega_\nu/\Omega_s$ , the ratio of the radial drift velocity to the sound speed, and  $\Omega_s/\Omega$ , the inverse timescale or the typical frequency associated with the sound speed in units of the angular velocity. In this section, we relate these parameters to the angular velocity profile  $\Omega(r)$  and the dynamical viscosity  $\nu\Sigma_0$  in the accretion disk. We then study the local excitation of the modes in the inner disk or boundary region where the hydrodynamic effects are important.

The ratio  $\kappa/\Omega$  of the epicyclic and orbital frequencies is related to the orbital frequency profile  $\Omega(r)$  through the relation

$$\frac{\kappa^2}{\Omega^2} = 4 \left(1 + \frac{1}{2} \frac{d \ln \Omega}{d \ln r}\right). \quad (40)$$

In a non-Keplerian boundary-transition region of the accretion disk around a neutron star that is a slow rotator,  $\Omega(r)$  is less than the Keplerian value  $\Omega_K(r)$ . Proceeding from the Keplerian outer disk through the transition region,  $\Omega(r)$  goes through a maximum and then decreases to match the star's rotation rate  $\Omega_*$  at the inner radius of the disk. The epicyclic frequency  $\kappa$ , degenerate with  $\Omega_K$  in the outer disk, increases through the transition region. The ratio  $\kappa/\Omega$  equals 2 at the radius where  $\Omega$  is maximum, has values between 1 and 2 in the outer parts of the non-Keplerian transition region, and is larger than 2 in the inner parts. Fig. 1 shows the run of  $\Omega(r)$  and  $\kappa(r)$  in a typical transition region. The numerical data for this example are obtained from the model curve shown in the panel (a) of Fig. 2 in Erkut & Alpar (2004).

For a viscous accretion disk, we write the turbulent viscosity,

$$\nu = \alpha \frac{c_s^2}{\Omega}, \quad (41)$$

using the  $\alpha$ -prescription (Shakura & Sunyaev 1973). The angular velocity profile in a disk depends on the radial profile of the vertically integrated dynamical viscosity,

$$\nu\Sigma_0 = \frac{\dot{M}}{3\pi} f(r), \quad (42)$$

and the appropriate boundary conditions. Here,  $f(r)$  is a dimensionless function for the dynamical viscosity. The run of  $f$  as a function of the radial distance in the typical disk-transition region is also shown in Fig. 1 (see Erkut & Alpar 2004). The radial profile of  $f$  is independent of the particular prescription for  $\nu$ . However, once we specify the kinematic viscosity as in equation (41), we can relate the surface density profile (see equation 17), using equations (41) and (42), to the orbital frequency profile and other parameters of the boundary region through

$$\beta = \frac{d \ln f}{d \ln r} + \frac{d \ln \Omega}{d \ln r} - 2 \frac{d \ln c_s}{d \ln r} \equiv \beta_0 - 2 \frac{d \ln c_s}{d \ln r}. \quad (43)$$

The first two terms, which we delineate as  $\beta_0$  characterize each of the boundary region models developed in Erkut & Alpar (2004), with values in the range  $-15 < \beta_0 < 3$ .

Using equations (7), (41), and (42), we obtain the explicit dependence of the ratio of the radial drift velocity and the sound speed on the disk-boundary region parameters as

$$\frac{\Omega_\nu}{\Omega_s} = -\frac{v_{r0}}{c_s} = \frac{3}{2} \left(\frac{\alpha}{f}\right) \frac{\Omega_s}{\Omega}. \quad (44)$$

Note that this ratio, for the given values of  $\alpha$  and  $\Omega_s/\Omega$ , takes its maximum value for the minimum value of  $f$ . As  $\Omega_\nu$ , which

determines the growth rates of the modes, depends on the ratio  $\Omega_s/\Omega$ , the growth rates differ for sufficiently large hydrodynamic corrections, i.e.,  $\Omega_s \lesssim \Omega$ , and the fastest growing modes can be identified. This is the regime of only slightly supersonic azimuthal flow. In a magnetic boundary layer or transition zone where  $\Omega < \Omega_K$ , the speed of sound can be written as  $c_s \simeq \Omega_K \sqrt{Hr}$  whereas in the weakly magnetized outer disk,  $c_s \simeq \Omega_K H$  (see Erkut & Alpar 2004). We therefore expect to find larger values for  $\Omega_s/\Omega$  in a non-Keplerian boundary region;  $\Omega_s/\Omega \simeq (\Omega_K/\Omega)(H/r)^{1/2}$ . The larger the ratio  $\Omega_s/\Omega$ , the stronger is the effect of hydrodynamic corrections on the growth rates of the modes.

We explore the run of the frequencies and the growth rates of free oscillations excited at a characteristic radius  $r$  in the innermost disk as the hydrodynamic parameter  $\Omega_s/\Omega$  changes at that radius. As a guideline, we have employed the model solutions of Erkut & Alpar (2004). These models qualitatively represent conditions in a boundary-transition region. The key model parameters can be easily translated into the parameters in equations (40), (43), and (44). The zeroth-order magnetic force in equation (23) can also be estimated from these model solutions with a range  $0 \leq \langle F_\phi^{\text{mag}} \rangle_0 / \nu_{r0} \Omega \lesssim 1$  in the inner boundary region. The maximum value of this parameter corresponds to the radius where  $\Omega$  is maximum. Near the innermost radius of the disk, the azimuthal magnetic force vanishes as the relative shear between the magnetosphere and the disk becomes negligible, i.e.,  $\Omega - \Omega_* \simeq 0$ .

To elucidate how the hydrodynamic parameters give different growth rates for different modes, we investigate the excitation of free oscillations in the typical boundary region shown in Fig. 1. To see the hydrodynamic effects on the growth rates of the modes, we use the full eigenfrequency solutions for axisymmetric and non-axisymmetric perturbations given in equations (A6)–(A8) and (A22)–(A24) (see Appendix). The panel (a) of Fig. 2 shows the real parts of the complex mode frequencies at the radius where  $\Omega$  is maximum for the  $m = 0$  and  $m = 1$  cases. For the boundary layer model chosen, the model parameters at this radius are  $\kappa/\Omega = 2$ ,  $\beta = -14$ ,  $f = 0.067$ , and  $\langle F_\phi^{\text{mag}} \rangle_0 / \nu_{r0} \Omega = 1$ . The panel (a) of Fig. 2 is obtained for  $\alpha = 0.1$ . Although the real parts of the mode frequencies do not change under a different value of the viscosity parameter, say  $\alpha = 0.01$  at this radius, the imaginary parts do (see panel b of Fig. 2). The unstable modes grow faster for  $\alpha = 0.1$  than they do for  $\alpha = 0.01$ , as shown in Fig. 2 (panel b). This is because the growth rates are primarily determined by  $\Omega_\nu/\Omega_s \propto \alpha/f$  (see equation 44). In Fig. 3, we display the real (panel a) and imaginary (panel b) parts of the mode frequencies at the innermost disk radius where  $\Omega = \Omega_*$  for  $m = 0$  and  $m = 1$ . The model parameters illustrated in Fig. 3 are  $\kappa/\Omega = 2.5$ ,  $\beta = -5$ ,  $f = 1$ , and  $\langle F_\phi^{\text{mag}} \rangle_0 / \nu_{r0} \Omega = 0$ . Fig. 3 is plotted for  $\alpha = 0.1$ . Note that the growth rates, for the same value of the viscosity parameter  $\alpha$ , are lower than those at the radius where  $\Omega$  is maximum.

The analysis for the particular transition zone discussed above can also be extended to other sample boundary regions with different model parameters. Our conclusion that the fastest growing modes are excited near the radius  $r = r_0$  where  $\Omega$  is maximum remains valid for all sub-Keplerian inner disks around slow rotators: The common property of all boundary regions is that the parameters  $|\beta|$  and  $\alpha/f$ , which determine the growth rates of the unstable modes, attain highest values near  $r_0$  where  $\kappa/\Omega \simeq 2$ . Note that the growing mode frequencies significantly exceed test-particle frequen-

cies in the boundary region for  $\Omega_s/\Omega \lesssim 1$ . In the limit of small hydrodynamic corrections ( $\Omega_s/\Omega \ll 1$ ), the mode frequencies converge to the corresponding test-particle frequencies (see panel a of Fig. 2 and panel a of Fig. 3) with negligible growth rates as expected (see panel b of Fig. 2 and panel b of Fig. 3).

The frequency branches that map to the test-particle frequencies  $\omega_1^{(0)} = \kappa$  and  $\omega_{1,2}^{(1)} = \kappa \pm \Omega$  in the limit of small hydrodynamic corrections,  $\Omega_s/\Omega \ll 1$ , have positive and rather fast growth rates at  $r \lesssim r_0$ , where  $\kappa/\Omega \gtrsim 2$ , when  $\Omega_s/\Omega \lesssim 1$  (see panel a of Fig. 2 and panel a of Fig. 3). We identify  $\omega_3^{(0)} = 0$  and  $\omega_3^{(1)} \simeq \Omega$  as the quasi-stable or decaying mode frequencies in the same range of  $\Omega_s/\Omega$  as shown in Fig. 2 (panel b) and Fig. 3 (panel b). Note that while each of the growing branches differs from test-particle frequencies as  $\Omega_s/\Omega$  increases, the difference frequency between consecutive bands is always  $\Delta\omega = \omega_1^{(1)} - \omega_1^{(0)} \lesssim \Omega$  or  $\Delta\omega = \omega_1^{(0)} - \omega_2^{(1)} \lesssim \Omega$  over a wide range of  $\Omega_s/\Omega$  (see panel a of Fig. 2 and panel a of Fig. 3). As  $\Omega \gtrsim \Omega_*$  in a boundary layer, we find  $\Delta\omega \simeq \Omega_*$  as observed for the relatively slow rotators among the neutron-star LMXBs that exhibit kHz QPOs.

#### 4. DISCUSSION AND CONCLUSIONS

We have studied the global hydrodynamic modes of long wavelength in the boundary or transition region of viscous accretion disks as a possible source of kHz QPOs in neutron-star LMXBs. The stability of the eigenmodes strongly depends on the global disk structure imposed by the boundary conditions as expected from the mode analysis in the long wavelength regime. Our local treatment takes account of the local effects of the global disk parameters on the excitation of hydrodynamic free oscillations.

We find that the frequencies and growth rates of the modes are mainly determined by global disk parameters such as  $\kappa/\Omega$ , the ratio of the radial epicyclic frequency to the orbital frequency, the radial surface-density profile  $\beta$ ,  $\Omega_\nu/\Omega_s$ , the ratio of the radial drift velocity to the sound speed, and  $\Omega_s/\Omega$ , the ratio of the sound speed to the azimuthal velocity. The local values of  $\kappa/\Omega$  and  $\beta$  directly follow from the global solution for the rotational dynamics of a boundary-transition region model. The parameters  $\Omega_\nu/\Omega_s$  and  $\Omega_s/\Omega$  depend additionally on the particular viscosity prescription and the details of the structure of accretion flow in the inner disk.

The hydrodynamic effects on the frequencies and growth rates of the modes are reflected by the parameters  $\Omega_\nu/\Omega_s$  and  $\Omega_s/\Omega$ . We have found that the growth rates of different modes for a given azimuthal wavenumber  $m$  differ significantly when the hydrodynamic corrections are sufficiently large, i.e.  $\Omega_\nu/\Omega_s \lesssim 1$  and  $\Omega_s/\Omega \lesssim 1$ . In this regime, the growing mode frequencies significantly exceed test-particle frequencies for a plausible range of  $\Omega_s/\Omega$  at any particular radius within the boundary region. This is because the effect of hydrodynamic corrections on the growth rates of the modes is expected to be strong in a magnetic boundary layer or transition zone as discussed in § 3.2. In the limit of small hydrodynamic corrections, i.e.  $\Omega_\nu/\Omega_s \ll 1$  and  $\Omega_s/\Omega \ll 1$ , the eigenmodes have test-particle frequencies with negligible growth rates. Our analysis shows that taking account of hydrodynamic effects has an important outcome: the frequencies of the growing modes gain higher values above test-particle frequencies as their growth rates increase for larger hydrodynamic corrections.

Throughout the boundary region, we have identified the growing mode frequencies by the eigenvalues that approach

the test-particle frequencies  $\omega_1^{(0)} = \kappa$ ,  $\omega_1^{(1)} = \kappa + \Omega$ , and  $\omega_2^{(1)} = \kappa - \Omega$  in the limit of small hydrodynamic corrections (see panel a of Fig. 2). Modes such as  $\omega_3^{(0)} = 0$  and  $\omega_3^{(1)} \simeq \Omega$  are not excited for the range of  $\Omega_s/\Omega$  in Fig. 2 (panel b) and Fig. 3 (panel b). The difference frequency between successive bands of growing modes is  $\Delta\omega \simeq \Omega_*$  as observed for the relatively slowly rotating neutron stars in LMXBs that show kHz QPOs (§ 3.2). In a boundary layer or transition region, the orbital frequency of the disk matter is close to the rotation frequency of the star ( $\Omega \sim \Omega_*$ ). As  $\Delta\omega \simeq \Omega$ , the separation between consecutive mode frequencies is always related to the spin frequency of the neutron star. This is the result of the boundary condition imposed by the rotating magnetosphere on the innermost disk. The modes of the test-particle frequencies  $\omega_1^{(0)} \simeq \kappa$  and  $\omega_2^{(1)} \simeq \kappa - \Omega$  were originally proposed by Alpar & Psaltis (2005) to be associated with the upper and lower kHz QPOs observed in neutron-star LMXBs. The frequency separation between the higher and lower-frequency kHz QPO peaks decreases by a few tens of Hz as both QPO frequencies increase by hundreds of Hz in a range of 200–1200 Hz per source in all observed sources, namely, Sco X-1, 4U 1608–52, 4U 1728–34 and 4U 1735–44 (van der Klis 2000). This pair of frequencies satisfies the observed behavior that the difference frequency  $\Delta\omega$  between two kHz QPOs decreases as both frequencies increase. According to our present analysis, the pairs of observed kHz QPO bands could be either  $\omega_1^{(1)} \simeq \kappa + \Omega$  and  $\omega_1^{(0)} \simeq \kappa$  or  $\omega_1^{(0)} \simeq \kappa$  and  $\omega_2^{(1)} \simeq \kappa - \Omega$ , respectively, since the identification of the observed QPOs with  $\omega_1^{(1)} \simeq \kappa + \Omega$  and  $\omega_1^{(0)} \simeq \kappa$  also meets the observed condition that  $\Delta\omega$  decreases when both QPO frequencies increase. The growth rates of free oscillations produce a wide spectrum of sidebands,  $\omega_{1,2}^{(m)} \simeq \kappa \pm |m|\Omega$ , some of which fall in the range of observed power spectra. The reduction to only two of kHz QPO bands as observed in neutron star sources must therefore be a product of forced oscillations, resonances, and boundary conditions. The role of forced oscillations and resonances in the excitation of particular modes will be discussed in future work.

We find that the fastest growing modes with frequency branches  $\kappa$  and  $\kappa \pm \Omega$  are excited near the disk radius  $r \lesssim r_0$ , where the orbital frequency is maximum. In the boundary layer, the loss of centrifugal support near  $r_0$  leads to some radial acceleration of the disk matter. The subsequent rise in the radial drift velocity of the disk matter is accompanied by a sudden drop in the surface density as the vertically integrated dynamical viscosity is minimized (see § 3.2). This picture is common to all boundary layers or transition zones for which magnetic braking is efficient (see Erkut & Alpar 2004 and references therein). Thus, independent of the boundary conditions and the magnetic field configuration in the boundary region, there exists a specific disk radius where the hydrodynamical background quantities such as the surface density  $\Sigma_0$  and the radial drift velocity  $v_{r0}$  change dramatically. The steepness in the change of the surface density in the radial direction is reflected through the parameter  $\beta$  (see equation 17). The sign and magnitude of  $\beta$  (the surface density profile in the disk) control whether the free oscillation modes will grow

or decay. We see that the modes of frequency bands  $\kappa$  and  $\kappa \pm \Omega$  can be excited with the largest growth rates only for the disk radii  $r \lesssim r_0$ , where  $\beta$  is minimum and  $\Omega$  is maximum (see § 3.2 for the range of  $\beta$ ). The inverse timescale,  $\Omega_\nu$ , associated with radial accretion also obtains its highest value near the same radii yielding the maximum growth rates in the accretion disk.

The boundary layers with sub-Keplerian rotation rates are usually expected to be realized in the innermost regions of accretion disks around *slow rotators*. For a *slow rotator*, the Kepler rotation rate at the inner disk radius  $\Omega_K(r_{in})$  prevails over the stellar rotation rate  $\Omega_*$ . As we have illustrated in § 3.2, the difference frequency between two consecutive bands of growing modes in the boundary region is close to the spin frequency of the neutron star ( $\Delta\omega \simeq \Omega_*$ ). This result agrees with the kHz QPO observations of the relatively slow rotators with spin frequencies below  $\sim 400$  Hz in neutron-star LMXBs. In these sources, for example, in 4U 1728–34, the lower kHz QPO frequencies increase from 600 to 900 Hz and the upper kHz QPO frequencies increase from 950 to 1200 Hz, while the difference between the two observed kHz QPO frequency bands decreases slightly, of the order of 10 Hz, while remaining still commensurate with the spin frequency of the neutron star (Méndez & van der Klis 1999). A second class of kHz QPO sources, such as the sources KS 1731–260, Aql X-1, 4U 1636–53, which have spin frequencies above  $\sim 400$  Hz is usually depicted as *fast rotators* (see Wijnands et al. 2003). In this second class of sources, for example in 4U 1636–53, the lower kHz QPO frequencies increase from 900 to 1150 Hz and the upper kHz QPO frequencies increase from 1150 to 1190 Hz, while the difference between the two observed kHz QPO frequency bands again decreases by amounts of the order of 10 Hz (see van der Klis 2000 and references therein). The frequency separation between the kHz QPOs is close to half the spin frequency of the neutron star if it is a *fast rotator*. The emergence of two seemingly different classes of neutron-star LMXBs could be related to whether the rotation rate of the neutron star is less or greater than that of the inner disk matter. It is probable that  $\Omega_* > \Omega_K(r_{in})$  for the relatively fast rotating neutron star sources for which the difference frequency between twin QPO peaks is  $\Delta\omega \simeq \Omega_*/2$ . Recent work by Méndez & Belloni (2007) actually suggests a more continuous distribution between  $\Delta\omega \simeq \Omega_*$  and  $\Delta\omega \simeq \Omega_*/2$ . The rotational dynamics of accretion flow in the innermost regions of accretion disks around these *fast rotators* could be quite different from those of the transition regions we consider here. We plan to address this issue in a subsequent paper.

We acknowledge support from the Marie Curie FP6 Transfer of Knowledge Project ASTRONS, MKTD-CT-2006-042722. M.H.E. was partially supported by a TÜBİTAK (The Scientific and Technical Research Council of Turkey) postdoctoral fellowship. D.P. was partially supported by NASA grant NAG-513374. M.A.A. acknowledges support from the Turkish Academy of Sciences and the Sabancı University Astrophysics and Space Forum.

#### APPENDIX

##### GENERAL EXPRESSIONS

The dispersion relation of the global force-free hydrodynamic modes we consider in § 3 is

$$(\omega - m\Omega) [(\omega - m\Omega)^2 - \Omega_a^2] - \Omega_b^3 - i [(\omega - m\Omega)^2 \Omega_c + \Omega_d^3] = 0, \quad (A1)$$

where

$$\Omega_a^2 \equiv \kappa^2 + [m^2 + \beta(1 + \beta)] \Omega_s^2 + [\beta(1 + \beta) - (1 + 2\beta)(1 - \gamma_\nu)] \Omega_\nu^2, \quad (\text{A2})$$

$$\Omega_b^3 \equiv 2m(1 + \beta) \Omega_s^2 \Omega + m\beta \Omega_s^2 \left( \frac{\kappa^2}{2\Omega} \right), \quad (\text{A3})$$

$$\Omega_c \equiv -(\gamma_\nu + 2\beta) \Omega_\nu, \quad (\text{A4})$$

and

$$\Omega_d^3 \equiv \beta \Omega_\nu \kappa^2 - \beta(1 + \beta)(1 - \gamma_\nu) \Omega_\nu^3 - (1 + \beta) [\beta(1 - \gamma_\nu) - m^2] \Omega_\nu \Omega_s^2. \quad (\text{A5})$$

Note that the solution of equation (A1), in the ideal case of an inviscid  $\Omega_\nu = 0$ , cold disk  $\Omega_s \simeq 0$ , where the gas particles barely interact with each other, is given by  $\omega_{1,2}^{(m)} \simeq m\Omega \pm \kappa$  and  $\omega_3^{(m)} \simeq m\Omega$ . In general, equation (A1), for the realistic case of  $\Omega_\nu \neq 0$  and  $\Omega_s \neq 0$ , yields

$$\omega_I^{(0)} = (\chi - \psi) \Omega_d + i \frac{\Omega_c}{3}, \quad (\text{A6})$$

$$\omega_{II}^{(0)} = \frac{1}{2}(\psi - \chi) \Omega_d + i \frac{\Omega_c}{3} + i \frac{\sqrt{3}}{2}(\chi + \psi) \Omega_d, \quad (\text{A7})$$

and

$$\omega_{III}^{(0)} = \frac{1}{2}(\psi - \chi) \Omega_d + i \frac{\Omega_c}{3} - i \frac{\sqrt{3}}{2}(\chi + \psi) \Omega_d \quad (\text{A8})$$

as the eigenfrequency solutions for axisymmetric perturbations ( $m = 0$ ), where

$$\psi \equiv \frac{1}{9\chi} \left( \frac{\Omega_c}{\Omega_d} \right)^2 - \frac{1}{3\chi} \left( \frac{\Omega_a}{\Omega_d} \right)^2, \quad (\text{A9})$$

$$\chi \equiv \left( i \frac{\eta_1}{4} + \frac{1}{2} \sqrt{\eta_2 - \eta_1} \right)^{1/3}, \quad (\text{A10})$$

$$\eta_1 \equiv 2 + \frac{2}{3} \left( \frac{\Omega_a^2 \Omega_c}{\Omega_d^3} \right) - \frac{4}{27} \left( \frac{\Omega_c}{\Omega_d} \right)^3, \quad (\text{A11})$$

and

$$\eta_2 \equiv 1 - \frac{4}{27} \left( \frac{\Omega_a}{\Omega_d} \right)^6 + \frac{1}{27} \left( \frac{\Omega_a^4 \Omega_c^2}{\Omega_d^6} \right). \quad (\text{A12})$$

For small hydrodynamic corrections,  $\eta_2 < \eta_1$ , we obtain

$$\text{Re} \left[ \omega_I^{(0)} \right] = \frac{(\sqrt{1 + \varepsilon_1} + \varepsilon_2)^{1/3} \Omega_a}{2} + \frac{(1 - \varepsilon_3) \Omega_a}{2(\sqrt{1 + \varepsilon_1} + \varepsilon_2)^{1/3}}, \quad (\text{A13})$$

$$\text{Im} \left[ \omega_I^{(0)} \right] = \frac{(\sqrt{1 + \varepsilon_1} + \varepsilon_2)^{1/3} \Omega_a}{2\sqrt{3}} - \frac{(1 - \varepsilon_3) \Omega_a}{2\sqrt{3}(\sqrt{1 + \varepsilon_1} + \varepsilon_2)^{1/3}} + \frac{\Omega_c}{3}, \quad (\text{A14})$$

$$\text{Re} \left[ \omega_2^{(0)} \right] = -\text{Re} \left[ \omega_1^{(0)} \right], \quad (\text{A15})$$

$$\text{Im} \left[ \omega_2^{(0)} \right] = \text{Im} \left[ \omega_1^{(0)} \right], \quad (\text{A16})$$

$$\text{Re} \left[ \omega_3^{(0)} \right] = 0, \quad (\text{A17})$$

$$\text{Im} \left[ \omega_3^{(0)} \right] = \Omega_c - 2 \text{Im} \left[ \omega_1^{(0)} \right] \quad (\text{A18})$$

as the only non-degenerate eigenfrequency solutions to the dispersion relation for axisymmetric perturbations, where

$$\varepsilon_1 \equiv \frac{27}{4} \left( \frac{\Omega_d}{\Omega_a} \right)^6 + \frac{9\Omega_c \Omega_d^3}{2\Omega_a^4} - \frac{\Omega_d^3 \Omega_c^3}{\Omega_a^6} - \frac{1}{4} \left( \frac{\Omega_c}{\Omega_a} \right)^2, \quad (\text{A19})$$

$$\varepsilon_2 \equiv \frac{3\sqrt{3}}{2} \left( \frac{\Omega_d}{\Omega_a} \right)^3 + \frac{\sqrt{3}\Omega_c}{2\Omega_a} - \frac{\sqrt{3}}{9} \left( \frac{\Omega_c}{\Omega_a} \right)^3, \quad (\text{A20})$$

and

$$\varepsilon_3 \equiv \frac{1}{3} \left( \frac{\Omega_c}{\Omega_a} \right)^2. \quad (\text{A21})$$



The general solutions to the dispersion equation for  $m \neq 0$  are

$$\omega_I^{(m)} = m\Omega + (\xi + \Lambda)\Omega_b + i\frac{\Omega_c}{3}, \quad (\text{A22})$$

$$\omega_{II}^{(m)} = m\Omega - \frac{1}{2}(\xi + \Lambda)\Omega_b + i\frac{\Omega_c}{3} + i\frac{\sqrt{3}}{2}(\xi - \Lambda)\Omega_b, \quad (\text{A23})$$

and

$$\omega_{III}^{(m)} = m\Omega - \frac{1}{2}(\xi + \Lambda)\Omega_b + i\frac{\Omega_c}{3} - i\frac{\sqrt{3}}{2}(\xi - \Lambda)\Omega_b, \quad (\text{A24})$$

where

$$\Lambda \equiv \frac{1}{3\xi} \left( \frac{\Omega_a}{\Omega_b} \right)^2 - \frac{1}{9\xi} \left( \frac{\Omega_c}{\Omega_b} \right)^2, \quad (\text{A25})$$

$$\xi \equiv \left( \frac{1}{2} + i\frac{\zeta_1}{4} + \frac{1}{2}\sqrt{\zeta_2 + i\zeta_1} \right)^{1/3} \quad (\text{A26})$$

$$\zeta_1 \equiv \frac{2}{3} \left( \frac{\Omega_a^2 \Omega_c}{\Omega_b^3} \right) + 2 \left( \frac{\Omega_d}{\Omega_b} \right)^3 - \frac{4}{27} \left( \frac{\Omega_c}{\Omega_b} \right)^3, \quad (\text{A27})$$

and

$$\zeta_2 \equiv 1 - \frac{4}{27} \left( \frac{\Omega_a}{\Omega_b} \right)^6 + \frac{1}{27} \left( \frac{\Omega_a^4 \Omega_c^2}{\Omega_b^6} \right) + \left( \frac{\Omega_d}{\Omega_b} \right)^6 - \zeta_1 \left( \frac{\Omega_d}{\Omega_b} \right)^3. \quad (\text{A28})$$

In the limit of small hydrodynamic corrections,  $|\zeta_1| \ll |\zeta_2|$ , we find

$$\text{Re} \left[ \omega_I^{(m)} \right] = m\Omega \pm \frac{\Omega_b \Omega_a}{|\Omega_b|} \mp \left( \frac{\Omega_c}{\Omega_a} \right)^2 \frac{|\Omega_b| \Omega_a}{6\Omega_b}, \quad (\text{A29})$$

$$\text{Im} \left[ \omega_I^{(m)} \right] = \frac{\Omega_c}{3} \left[ 1 \pm \left( \frac{\Omega_c}{\Omega_a} \right) \frac{|\Omega_b|}{2\sqrt{3}\Omega_b} \right], \quad (\text{A30})$$

$$\text{Re} \left[ \omega_2^{(m)} \right] = m\Omega \mp \frac{\Omega_b \Omega_a}{|\Omega_b|} \pm \left( \frac{\Omega_c}{\Omega_a} \right)^2 \frac{|\Omega_b| \Omega_a}{6\Omega_b}, \quad (\text{A31})$$

$$\text{Im} \left[ \omega_2^{(m)} \right] = \text{Im} \left[ \omega_I^{(m)} \right], \quad (\text{A32})$$

$$\text{Re} \left[ \omega_3^{(m)} \right] = m\Omega, \quad (\text{A33})$$

$$\text{Im} \left[ \omega_3^{(m)} \right] = \Omega_c - 2 \text{Im} \left[ \omega_I^{(m)} \right] \quad (\text{A34})$$

as the only non-degenerate eigenfrequency solutions to the dispersion relation for non-axisymmetric perturbations.

#### REFERENCES

- Abramowicz, M. A., Karas, V., Kluźniak, W., Lee, W. H., & Rebusco, P. 2003, PASJ, 55, 467
- Alpar, M. A., Hasinger, G., Shaham, J., & Yancopoulos, S. 1992, A&A, 257, 627
- Alpar, M. A., & Psaltis, D. 2005, preprint (astro-ph/0511412)
- Alpar, M. A., & Yılmaz, A. 1997, NewA, 2, 225
- Erkut, M. H., & Alpar, M. A. 2004, ApJ, 617, 461
- Kato, S. 2001, PASJ, 53, 1
- Méndez, M., & Belloni, T. 2007, MNRAS, 381, 790
- Méndez, M., & van der Klis, M. 1999, ApJ, 517, L51
- Miller, M. C., Lamb, F. K., & Psaltis, D. 1998, ApJ, 508, 791
- Psaltis, D., Belloni, T., & van der Klis, M. 1999, ApJ, 520, 262
- Psaltis, D., & Norman, C. 2000, preprint (astro-ph/0001391)
- Shakura, N. I., & Sunyaev, R. A. 1973, A&A, 24, 337
- Stehle, R., & Spruit, H. C. 1999, MNRAS, 304, 674
- Stella, L., Vietri, M., & Morsink, S. M. 1999, ApJ, 524, L63
- van der Klis, M. 2000, ARA&A, 38, 717
- Wagoner, R. W. 1999, Phys. Rep., 311, 259
- Wijnands, R., van der Klis, M., Homan, J., Chakrabarty, D., Markwardt, C. B., & Morgan, E. H. 2003, Nature, 424, 44

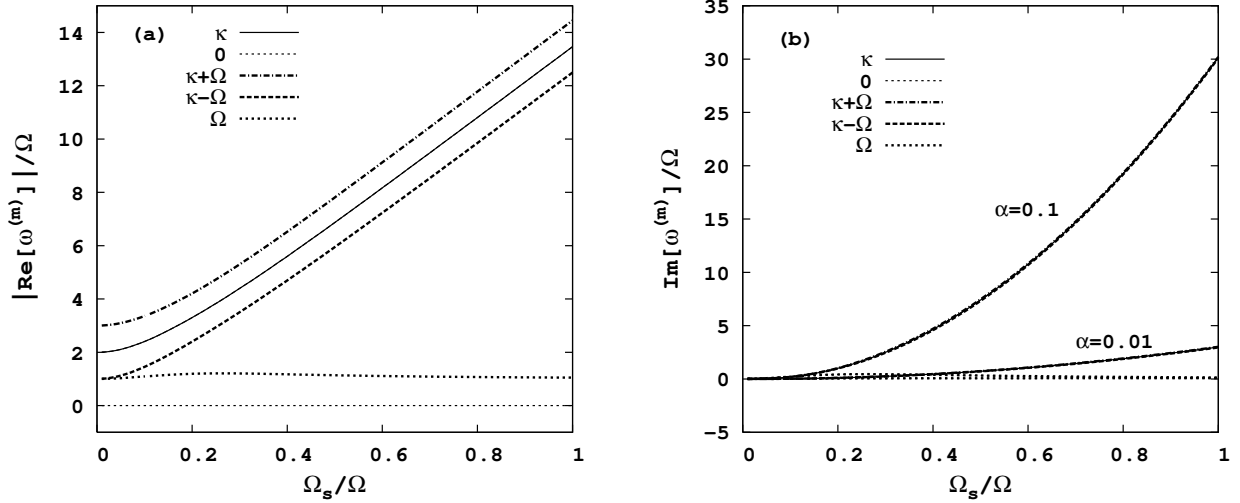


FIG. 2.— The real and imaginary parts of the solutions to the dispersion relation for axisymmetric ( $m=0$ ) and non-axisymmetric ( $m=1$ ) perturbations excited at the radius where the orbital frequency  $\Omega$  is maximum. The model parameters are  $\kappa/\Omega=2$ ,  $\beta=-14$ ,  $f=0.067$ , and  $\langle F_\phi^{\text{mag}} \rangle_0/v_{r0}\Omega=1$ . The curves are labelled with the values of the frequencies in the test-particle limit. The  $\kappa$  and  $\kappa \pm \Omega$  modes have the same positive growth rates, growing more rapidly for larger  $\alpha$ . The zero-frequency and  $\Omega$  modes, indicated by the overlapping dotted curves, do not grow for any  $\alpha$ .

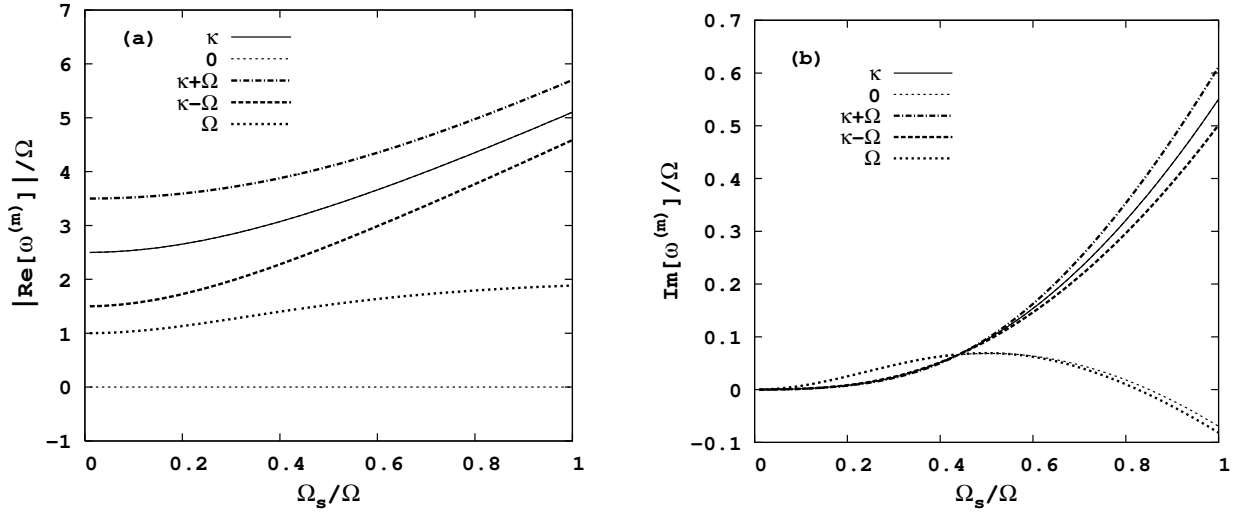


FIG. 3.— The real and imaginary parts of the solutions to the dispersion relation for axisymmetric ( $m=0$ ) and non-axisymmetric ( $m=1$ ) perturbations excited at the innermost disk radius where  $\Omega = \Omega_*$ . The model parameters are  $\kappa/\Omega=2.5$ ,  $\beta=-5$ ,  $f=1$ , and  $\langle F_\phi^{\text{mag}} \rangle_0/v_{r0}\Omega=0$ . The frequencies and growth rates are obtained for  $\alpha=0.1$ . The growing modes are associated with the  $\kappa+\Omega$ ,  $\kappa$ , and  $\kappa-\Omega$  branches, with  $\kappa+\Omega$  having the highest growth rate. The zero-frequency and  $\Omega$  modes grow for lower values of  $\Omega_s/\Omega$ , but decay in the regime of  $\Omega_s/\Omega \lesssim 1$ , where the  $\kappa$  and  $\kappa \pm \Omega$  modes have the fastest growth rates.